Modeling the feedback between aerosol and meteorological variables in the atmospheric boundary layer during a severe fog-haze event over the North China Plain

Yi Gao[1], Meigen Zhang*[,1], Zirui Liu[1], Lili Wang[1], Pucai Wang[2], Xiangao Xia[2], and Minghui Tao[3]

[1]*State Key Laboratory of Atmospheric Boundary Layer Physics and Atmospheric Chemistry (LAPC), Institute of Atmospheric Physics, Chinese Academy of Sciences, Beijing, China*
[2]*Key Laboratory of Middle Atmosphere and Global Environment Observation (LAGEO), Institute of Atmospheric Physics, Chinese Academy of Sciences, Beijing, China*
[3]*State Key Laboratory of Remote Sensing Science, Institute of Remote Sensing and Digital Earth, Chinese Academy of Sciences, Beijing, China*

*Corresponding author:

Meigen Zhang
State Key Laboratory of Atmospheric Boundary Layer Physics and Atmospheric Chemistry (LAPC)
Institute of Atmospheric Physics
Chinese Academy of Sciences
Huayanli 40#, Chaoyang District, Beijing, China, 100029

Tel: 010-62040159(o)
E-mail: mgzhang@mail.iap.ac.cn

Abstract

The feedback between aerosol and meteorological variables in the atmospheric boundary layer over the North China Plain (NCP) is analyzed by conducting numerical experiments with and without the aerosol direct and indirect effects via a coupled meteorology and aerosol/chemistry model (WRF-Chem). The numerical experiments are performed for the period 2–26 January 2013, during which a severe fog-haze event (10–15 January 2013) occurred with the simulated maximum hourly surface $PM_{2.5}$ concentration of ~600 ug m^{-3}, minimum atmospheric visibility of ~0.3 km and 10–100 hours of simulated hourly surface $PM_{2.5}$ concentration above 300 ug m^{-3} over NCP. Comparison of model results with aerosol feedback against observations indicates that the model can reproduce the spatial and temporal characteristics of temperature, relative humidity (RH), wind, surface $PM_{2.5}$ concentration, atmospheric visibility, and aerosol optical depth reasonably well. Analysis of model results with and without aerosol feedback shows that during the fog-haze event aerosols lead to a significant negative radiative forcing of -20–-140 W m^{-2} at the surface and a large positive radiative forcing of 20–120 W m^{-2} in the atmosphere and induce significant changes in meteorological variables with maximum changes during 09:00-18:00 (LT) over urban Beijing and Tianjin, and south Hebei Province: the temperature decreases by 0.8–2.8 ℃ at the surface and increases by 0.1–0.5 ℃ at around 925 hPa while the RH increases by about 4–12% at the surface and decreases by 1–6% at around 925 hPa. As a result, the aerosol-induced equivalent potential temperature profile change shows that the atmosphere is much more stable and thus the surface wind speed decreases by up to 0.3 m s^{-1} (10%) and the atmosphere boundary layer height decreases by 40–200 m (5–30%) during the daytime of

this severe fog-haze event. Owing to this more stable atmosphere, during 09:00–18:00, 10–15 January, compared to the surface $PM_{2.5}$ concentration from the model results without aerosol feedback, the average surface $PM_{2.5}$ concentration increases by 10–50 μg m^{-3} (2–30%) over Beijing, Tianjin, and south Hebei province and the maximum increase of hourly surface $PM_{2.5}$ concentration is around 50 μg m^{-3} (70%), 90 μg m^{-3} (60%) and 80 μg m^{-3} (40%), averaged over Beijing, Tianjin and south Hebei Province, respectively. Although the aerosol concentration is maximum at nighttime, the mechanism of feedback by which meteorological variables increase the aerosol concentration most occurs during the daytime (around 10:00 and 16:00). The results suggest that aerosol induces a more stable atmosphere, which is favorable for the accumulation of air pollutants, and thus contributes to the formation of fog-haze events.

1. Introduction

The occurrence of fog-haze events has been more frequent in recent years in the developing regions and mega-cities of China. These regions, as determined by visibility observations from the China Meteorological Administration (CMA) (Che et al., 2007, 2009b; Zhang et al., 2012), include: the North China Plain (NCP: Beijing, Tianjin, Hebei Province, Shanxi Province, and part of Inner Mongolia Province) and Guanzhong Plain, East China – mainly the Yangtze River Delta area, South China – mostly in the areas of Guangdong and the Pearl River Delta, and the Sichuan Basin in Southwest China. The North China Plain (NCP) is one of China's most important social and economic regions; it has a huge population and undergone rapid development during recent decades. Large emission sources emit primary aerosols and the precursors of secondary aerosols (Zhang et al., 2009; Street et al., 2003), resulting in high loads of aerosols and many aerosol species [e.g. sulfate (SO_4^{2-}), nitrate (NO_3^-), ammonium (NH_4^+), black carbon (BC), organic carbon (OC), and dust] over the NCP. This is the main reason for the deterioration of visibility and fog-haze events through light extinction (Sun et al., 2006; Chan and Yao, 2008). Based on observational studies (Cheng et al., 2011; Zhao et al., 2013, Quan et al., 2011), during haze periods, the concentration of particulate matter is much higher than on normal days, and fine-mode aerosol is predominant on haze days. Using the RAMS (Regional Atmospheric Modeling System) – CMAQ (Community Multi-scale Air Quality) modeling system (RAMS–CMAQ), Han et al. (2013) showed that the low visibility in December 2010 over the NCP was primarily caused by a high mass burden of $PM_{2.5}$ as a result of local pollutant accumulation, long-range transport,

and SO_4^{2-} and NO_3^-, which are the two major inorganic aerosol components of $PM_{2.5}$, decreasing visibility by contributing 40% to 45% of the total extinction coefficient value.

During 10–15 January 2013, extremely severe fog-haze occurred over the NCP, especially over Beijing, Tianjin, and south of Hebei Province with very high aerosol concentration and extremely low atmospheric visibility. The $PM_{2.5}$ (particulate matter of 2.5μm or less in aerodynamic diameter) concentration at Beijing were 300–800 μg m^{-3} and the air quality index (AQI) was >300 (AQI above 300 is considered hazardous to all humans), according to data provided by the Ministry of Environmental Protection (MEP) of China. This month has been reported as the haziest month of the past 60 years in Beijing, and the reason for its formation draws much attention and is the focus of many studies (e.g. H. Wang et al., 2014; Y. S. Wang et al., 2014; Sun et al., 2014; Zhang et al., 2014; Che et al., 2014; Tao et al., 2014). By analyzing observations from the Campaign on the Atmospheric Aerosol Research Network of China (CARE-China), Y. S. Wang et al. (2014) showed that during 9–15 January 2013, the hourly surface $PM_{2.5}$ concentration reached 680 μg m^{-3} in Beijing, Shijiazhuang (the capital city of Hebei Province), and Tianjin. It was indicated that a synoptic scale stagnation, unusually cold air, and local metrological conditions (which were extremely unfavorable for the diffusion of air pollutants) were the external reasons, while the rapid transfer from aerosol precursor to aerosol was the main internal reason, for this fog-haze event (Y. S. Wang et al., 2014). Sun et al. (2014) showed that the PM_1 mass concentration during 10–14 January in Beijing ranged from 144–300 μg m^{-3}, which was 10 times higher than that during clean periods. They also concluded that stagnant meteorological conditions, coal combustion,

secondary production, and regional transport were the four main factors driving the formation and evolution of haze pollution in Beijing during wintertime.

It is known that atmospheric aerosols enhance the absorption and scattering of radiation (direct effect, DE) and act as cloud condensation and ice nuclei that alter cloud properties and precipitation (indirect effect, IE) (Twomey, 1974; Albrecht, 1989). These in turn lead to large decreases in solar radiation reaching the earth's surface, increases in solar heating of the atmosphere, and changes in the distribution of atmospheric temperature structure and precipitation (Ramanathan et al., 2001). It was shown that aerosol DE at the surface was 32.8 W m^{-2} at Xianghe, a suburban site in the NCP, which was comparable to that of cloud radiative effect (Li et al., 2007; Xia et al., 2007). Analysis of a heavy pollution episode in fall of 2004 over northern China showed that the instantaneous aerosol DE at the surface reached 350 W m^{-2} and 300 W m^{-2} of which was absorbed by the atmosphere, therefore, a more stable atmosphere was expected (Liu et al., 2007). Many modeling studies have indicated a decrease in the seasonal/annual average temperature at the surface induced by aerosol over China (Qian et al., 2003; Liu et al., 2010; Wu and Han, 2011; Huang et al., 2006). Wu et al. (2009) used the CAM (Community Atmosphere Model) to simulate the DE of aerosol (SO_4^{2-}, dust, BC, and OC) on temperature during 1960–2000 and showed that the surface temperature decreased by about 1.5 K, while atmospheric temperature decreased under 850 hPa and increased in the middle troposphere.

Most of the aforementioned studies focused only on the impacts of meteorological condition on air quality or aerosol-induced meteorological condition changes on climate scale, ignoring the feedback from aerosol-induced meteorological conditions change to

aerosol concentration and the change of meteorological variables over shorter time scales (e.g. the diurnal cycle). These may affect the evolution of air pollution, which usually operates over such shorter time scales. In this paper, we estimate the feedback between aerosols and meteorological variables in the atmospheric boundary layer over the NCP during the fog-haze event of 10–15 January 2013 by conducting numerical simulations using a coupled meteorology and aerosol/chemistry model (WRF-Chem). We begin by introducing the Weather Research and Forecasting-Chemistry model (WRF-Chem), the handling of emissions and the numerical experiments in section 2, followed by a description of the observation data in section 3. Next, we present the model results in section 4: the performance of WRF-Chem in simulating the meteorological variables, surface $PM_{2.5}$ concentrations, visibility, and aerosol optical depth (AOD) over the NCP; the aerosol impacts on temperature, relative humidity (RH), energy budget, the equivalent potential temperature (EPT) profile, wind, and atmospheric (planetary) boundary layer height (PBLH) during the fog-haze event over the NCP; and the feedback of the above meteorological variables changes to aerosol concentrations. Finally, a summary of the key findings is given in section 5.

2. Model description

2.1 WRF-Chem Model

WRF-Chem is a version of the Weather Research and Forecasting (WRF) model (Skamarocket al., 2008) that simulates trace gases and aerosol simultaneously with the meteorological fields (Grell et al., 2005). The version used in this study is based on v3.2.1, but with updates including the GOCART (Georgia Tech/Goddard Global Ozone

Chemistry Aerosol Radiation and Transport) dust emission coupled with MOSAIC (Model for Simulating Aerosol Interactions and Chemistry) (Zhao et al., 2010), and representation of aerosol direct radiative feedback in the Rapid Radiative Transfer Model for GCMs (RRTMG) radiation (Zhao et al., 2011), which were released in v3.3. All major components of aerosol are treated in the model, including SO_4^{2-}, NO_3^-, NH_4^+, BC, OC, sea salt, mineral dust, and aerosol water. Different aerosol species are internally mixed within the mode and externally mixed among different modes. The aerosol scheme includes the representation of physical and chemical processes of emission, nucleation, condensation, coagulation, aqueous-phase chemistry, water uptake by aerosols, and dry and wet deposition. Aerosol optical properties such as extinction, single-scattering albedo, and asymmetry factor for scattering are computed as a function of wavelength and three-dimensional position. Each chemical constituent of the aerosol is associated with a complex refraction index calculated by volume averaging for each size bin (or mode), and Mie theory is used to compute the extinction efficiency (Qe) and the scattering efficiency (Qs). To efficiently compute Qe and Qs, WRF-Chem uses a methodology described by Ghan et al. (2001a) in which the full Mie calculations are first performed to obtain a table of seven sets of Chebyshev expansion coefficients, but later are skipped and Qe and Qs are calculated using bilinear interpolation over the Chebyshev coefficients stored in the table. A detailed description of the computation of aerosol optical properties in WRF-Chem can be found in Fast et al. (2006) and Barnard et al. (2010). Bulk hygroscopicity of each size mode/bin, equivalent to *k* in Petters and Kreidenweis (2007), is based on the volume-weighted average of the hygroscopicity of each aerosol component. The aerosol wet radius is calculated based on Kohler theory. Aerosol–cloud

interactions for the aerosol first and second IEs are included in the model by Gustufson et al. (2007) for calculating the activation and resuspension between interstitial aerosols and cloud droplets, which is similar to the method used in the MIRAGE (Model for Integrated Research on Atmospheric Global Exchanges) general circulation model (Ghan et al., 2001b). Aerosol activation is parameterized in terms of updraft velocity and the properties (number, size and hygroscopicity) of all of the aerosol modes (Abdul-Razzak and Ghan, 2000). The autoconversion of cloud water to rain water depends on cloud droplet number, following Liu et al. (2005).

2.2 Numerical experiments and emissions

In this study, WRF-Chem is configured to cover the east part of China (101 °–134 °E, 25 °–46 °N) with 80 (S–N) ×90 (W–E) grid points at 27 km horizontal resolution centering on Central China (117 °E, 36 °N), and 51 vertical layers up to 50hPa with 25 layers under 850 hPa. Figure 1 shows the study domain used in this paper. The Morrison two-moment bulk microphysics scheme is used to include the aerosol IE (Gustafson et al., 2007) and the RRTMG longwave/shortwave scheme is used to include the aerosol DE (Zhao et al., 2011). The CBMZ (carbon bond mechanism) and MOSAIC (Model for Simulating Aerosol Interactions and Chemistry) (Zaveri et al., 2008; Fast et al., 2006) are used in this study. MOSAIC uses a sectional approach where the aerosol size distribution is divided into discrete size bins defined by their lower and upper dry particle diameters. In this study, the aerosol size is divided into eight bins. The initial meteorological fields and boundary conditions are from the National Centers for Environmental Prediction (NCEP) Final Reanalysis data. Both the initial and boundary chemical conditions are from

MOZART's (Model for OZone and Related chemical Tracers) chemical boundary conditions which are specific to the period being studied.

The simulation is conducted from 14 December 2012 to 26 January 2013, including the time for model spin-up. Two numerical experiments are conducted in order to investigate the feedback between aerosol and meteorological variables. The baseline experiment (EXP_CTL) is conducted by the WRF-Chem model with standard anthropogenic emissions (see section 2.3) and full coupling of aerosol and meteorology simulation. The sensitivity experiment (EXP_NOEF) is conducted by closing the feedback between aerosol and meteorological variables, i.e. eliminating the aerosol DE and IE in the model. The effect of aerosol on meteorological variables and the feedback of the aerosol-induced meteorological variables changes to aerosol concentrations can be estimated as the difference between EXP_CTL and EXP_NOEF. The model results from EXP_CTL during 2–26 January 2013 are used for the model evaluation, while the difference between the numerical experiment results from 10–15 January 2013, the fog-haze period, is analyzed to study aerosol feedback effects.

2.3 Emissions

Anthropogenic emissions of carbon monoxide (CO), nitrogen oxides (NOx), SO_2, volatile organic compounds (VOCs), BC, OC, $PM_{2.5}$, and PM_{10} are based on Tsinghua University's 2010 monthly emission inventory (Lei et al., 2011, Zhang et al., 2009, and He et al., 2012), and are added to the diurnal information based on Wang et al. (2010). We use the 2010 NH_3 emission from the Regional Emission inventory for the Asia domain (REAS, http://www.jamstec.go.jp/frsgc/research/d4/emission.htm). Biomass-burning emission is obtained from the Global Fire Emissions Database, Version

3 (GFEDv3) with monthly temporal resolution (Randerson et al., 2005). Biogenic emission is from the Model of Emission of Gases and Aerosol from Nature (MEGAN) (Guenther et al., 2006). Dust emission is calculated online following Zhao et al. (2010). Sea salt emission is calculated online following Gong et al. (1997) in the publically released version of WRF-Chem. In this study, the sea salt emission scheme is updated following Gong (2003) to include the correction of particles with radius less than 0.2 μm, and Jaeglé et al. (2011) to include the sea salt emission dependence on sea surface temperature.

3. Observation data

The monitoring of meteorological data and visibility from the surface stations of the Chinese National Meteorological Center (CNMC; http://cdc.cma.gov.cn/home.do) were collected to evaluate the performance of the meteorological field simulation. CNMC has 726 measurement stations that are evenly distributed throughout mainland China and has been providing long-term surface observations of several meteorological variables since 1 January 1951 (Feng et al., 2004). The sites used in the study include: BJ (54511, Beijing, 39.8°N, 116.47°E), MY (54416, Miyun, 40.38°N, 116.87°E), BD (54602, Baoding, 38.85°N, 115.52°E), TS (54534, Tangshan, 39.07°N, 118.15°E), TJ (54527, Tianjin, 39.08°N, 117.07°E), QHD (54449, Qinhuangdao, 39.85°N, 119.52°E), and SJZ (53698, Shijiazhuang, 38.03°N, 114.42°E). Each site is denoted as a circle in Fig. 1.

The surface $PM_{2.5}$ concentrations from 2–26 January 2013 are from the CARE-China network (Y. S. Wang et al., 2014), which is located in the Jing-Jin-Ji area. The sites include BJ (Beijing, 39.97°N, 116.37°E), XL (Xinglong, 40.39°N, 117.58°E), XH

(Xianghe, 39.75 °N, 116.96 °E), and TJ (Tianjin, 39.08 °N, 117.21 °E), of which BJ and TJ are urban sites, XH is a suburban site, and XL is considered as the background area of the NCP. Observational sites in the CARE-China network are equipped with RP1400-$PM_{2.5}$ or RP1405-$PM_{2.5}$ (ThermoScientific: http://www.thermoscientic.com), which provide a continuous direct mass measurement of particulates by utilizing a tapered element oscillating microbalance (TEOM) (Patashnick and Rupprecht, 1991). Each site is denoted as a star in Fig. 1.

The Aerosol Robotic Network (AERONET) (Holben et al., 1998) is a network of sun- and sky-scanning ground-based automated radiometers providing data on aerosol optical properties (Dubovik and King, 2000; Dubovik et al., 2002). In this study, we use the Level 2.0 AOD data in 2013. The three sites are BJ [Beijing, 39.98 °N, 116.38 °E, 30 m.s.l.(Mean Surface Level)], XL (Xinglong, 40.39 °N, 117.58 °E, 940 m.s.l.), and XH (Xianghe, 39.75 °N, 116.99 °E, 80 m.s.l.), which have the same locations as the sites in the CARE-China network.

AOD data at Huimin site (37.48 °N, 117.53 °E, 11.7 m.s.l.) from Che et al. (2014) which is collected from the China Aerosol Remote Sensing Network (CARSNET) and were processed using the ASTPwin software offered by Cimel Ltd. Co (Che et al., 2009a) is also used. This site is denoted as a cross in Fig.1.

The Moderate Resolution Imaging Spectroradiometer (MODIS) aboard the Terra and Aqua satellites covers eastern China twice a day at around 1100 and 1300 local time, respectively. The Collection 6 MODIS enhanced Deep Blue algorithm provides 10 km aerosol data over all cloud-free land surfaces except for snow-covered regions with expected errors within 0.05±20% (Hsu et al., 2013). The improved cloud mask method

allows more aerosol retrievals in heavy aerosol loading conditions, making Collection 6 MODIS aerosol data more suitable for monitoring haze pollution in eastern China.

4. Results and discussion

4.1 Model result for meteorological variables, surface $PM_{2.5}$ concentration, visibility, and aerosol optical depth

In this section, a comparison between the model results for temperature, RH, wind, surface $PM_{2.5}$ concentration, visibility, and AOD from EXP_CTL and observations during 2–26 January 2013 is presented. Figure 2 are the time series of observed and simulated daily-averaged surface temperature, surface RH, precipitation, surface wind speed, and wind direction at BJ, MY, BD, TS, TJ, and QHD during 2–26 January 2013, respectively. The corresponding statistical analysis of the comparisons between simulated and observed temperature, RH, and wind is presented in Table 1. As seen in Fig. 2, the simulated meteorological variables agree well with observations. For the temperature, the model can depict its temporal variation but slightly underestimates the values at BJ and TJ, with correlation coefficients (R) of 0.78–0.91 and mean bias (MB) of −1.6 ℃ to 0.5 ℃ at the six sites. The model also reproduces the spatial distribution of temperature: the temperature is minimum at MY and QHD, of which MY is at the highest latitude and QHD is a coastal site (Fig. 1); while the maximum is at BJ and TJ, which are both urban sites located in big cities. The observed RH is also reasonably reproduced by the model (R = 0.72–0.90; MB = −10.0% to −8.8%). During 10–15 January, both the simulated and observed RH are very high, with values ranging from 70% to 90%, especially at BD, TS, TJ, and QHD, which may be influenced by the south and southeast wind flow from more

moist areas (Gao et al., 2014). The high RH over the NCP will contribute to the high aerosol concentration and fog-haze event during 10–15 January (Zhang et al., 2014). From Fig. 2, the model also reproduces the precipitation during 20–21 January but underestimates the values of daily precipitation. This may be due to the relatively coarse model resolution (27 km) that is unable to resolve the local variability at each site. There is no precipitation during the fog-haze period (10–15 January). The simulated variation of the maximum and mean wind speed and wind direction in the model agree well with the observation at the six sites (R = 0.51–0.83 for mean wind speed and 0.22–0.86 for wind direction). However, the model overestimates the mean wind speed by 0.5–1.9 m s^{-1} at the six sites. This may be due to the out-of-date land surface data in the model which is adopted from 5 min resolution USGS (United States Geological Survey) 24 category data derived from 1 km Advanced Very High Resolution Radiometer (AVHRR) measurement in a 12-month period spanning from April 1992 to March 1993 (Loveland et al., 1991; Brown et al., 1993). The USGS datasets may underestimate the urbanization over NCP comparing with present-day land surface data (Yu et al., 2012). The maximum wind speed is simulated much better by the model than the mean wind speed [R = 0.60–0.76, normalized mean bias (*NMB*) = 6%–20%]. The reason may be that the simulated wind speed is instantaneous while the observed mean wind speed is ten-minutes averaged. In addition, the out-of-data land surface data make the small wind speed cannot be well reproduced by model.

Figure 3 shows the time series of hourly surface $PM_{2.5}$ concentration from the observation and the corresponding model results from EXP_CTL at BJ, XL, XH, and TJ during 2–26 January 2013. The statistical analysis between the model results and

observation of surface $PM_{2.5}$ concentration is shown in Table 1. In general, the model reasonably reproduces the hourly variation of surface $PM_{2.5}$ concentration during 2–26 January at the four sites (R = 0.56–0.69, NMB = −10.9%–59.5%). Both the observation and model results show the surface $PM_{2.5}$ concentration to be highest at XH and TJ, of which XH is a suburban site located in Hebei Province and TJ is an urban site located in Tianjin. Note that although XH is a suburban site, the surface $PM_{2.5}$ concentration at this site is comparable to, or even higher than, that at BJ (Fig. 3 and Table 1), which may suggest more pollutants over the south part of Hebei Province and transport of pollution to Beijing. The surface $PM_{2.5}$ concentration is lowest at XL, which is a background site located at the top of a mountain (940 m.s.l.) and less affected by anthropogenic activities and more affected by transport compared to other sites. The simulated surface $PM_{2.5}$ concentration agrees very well with the observation at XL (R = 0.69), indicating that the atmospheric transport process is reproduced by the model. The model overestimates the surface $PM_{2.5}$ concentration at XH and TJ. In Fig. 3, focusing on the fog-haze period (10–15 January), it can be seen that the event starts from midnight on 10 January, with the surface $PM_{2.5}$ concentration rising from around 100 to 200–300 μg m^{-3} at BJ, from around 50 to 200–300 μg m^{-3} at XL, and from 100 to 200–400 μg m^{-3} at XH and TJ. After that, the concentration continues to increase to 200–400 μg m^{-3} at BJ and XL, and to 300–500 μg m^{-3} at XH and TJ, during the daytime of 11 January. The surface $PM_{2.5}$ concentration decreases during the night on 11 January at BJ and XL, but maintains a high value of 200–500 μg m^{-3} at XH and TJ. The surface concentration increases again on 12 and 13 January, with a value of 200–400 μg m^{-3} at BJ, 100–200 μg m^{-3} at XL, and 200–500 μg m^{-3} at XL and TJ. During the nighttime of 14 January, the surface $PM_{2.5}$

concentration begins to decrease to around 50–100 μg m^{-3} at all four sites. The consistent variation of surface $PM_{2.5}$ concentration at the four sites and the rapid rise of surface $PM_{2.5}$ concentration at XL suggest that the fog-haze event of 10–15 January 2013 was regionally distributed.

Figure 4 is the time series of hourly visibility at 00:00, 06:00, 12:00 and 18:00 from CNMC measurements and the corresponding WRF-Chem simulation at BJ, TJ, BD, and SJZ during 2–26 January 2013. The visibility is calculated as 3.912/aerosol extinction coefficient at 550nm. The impacts of gas phase molecules on visibility include Rayleigh scattering of air, and the absorptions of O_3, NO_2, and SO_2 of solar radiation are small compared with the droplets and particles under heavy aerosol loading conditions. As a result, their effects on visibility are ignored in this study (Deng et al., 2008; Quan et al., 2011). The simulated aerosol extinction coefficient at 550nm is calculated by using the default output AOD and Angstrom exponent derived from the output AODs at 400nm and 600nm. Therefore, the evaluation of the modeled visibility also reflects the evaluation of the modeled aerosol concentration and optical properties. From Fig. 4 and Table 1, the visibility is reproduced well by the model (R = 0.77, 0.66, 0.58, and 0.43 and MB = 5.0, 0.1, 0.7, and -0.2 km at the four sites, respectively). The model overestimates the visibility at BJ, and the overestimation is mainly due to the overestimation of visibility on clear days. This may be caused by the bias of the modeled extinction coefficient and aerosol mass concentration. Nevertheless, the model is able to capture the deterioration of visibility on polluted days at the four sites. Both the observation and model results show the value of visibility to be very low (around 1–3 km) during 10–14

January. However, the model overestimates the visibility at BJ on 12 January, which may be due to the underestimated surface $PM_{2.5}$ concentration on 12 January (Fig. 3).

Figure 5 is the time series of daily AOD at 550 nm from the AERONET measurements at BJ, XL, and XH and Che et al. (2014) at Huimin site and MODIS deep-blue AOD retrievals and the corresponding WRF-Chem simulation during 2–26 January 2013. The simulated AOD at 550nm is calculated by using the Angstrom exponent derived from the default output AODs at 400nm and 600nm. As the MODIS aboard the Aqua satellites covers eastern China at around 13:00 local time, the simulated AOD at 13:00 is showed in Figure 5. Statistical analysis of the comparison between the simulated and observed daily AOD from AERONET is presented in Table 1. As seen in Fig. 5, the model also reasonably reproduces the day-to-day variations of the observed AOD by AERONET and MODIS, although there are several missing data; the *R* values between the simulated and observed AODs from AERONET are 0.59, 0.99, 0.60 and 0.74 for the BJ, XL, XH and Huimin sites, respectively. The AOD from MODIS is much higher than that from AERONET, indicating that the AOD may be overestimated by MODIS. The modeled averaged AOD is higher at XH and lower at XL, consistent with the surface $PM_{2.5}$ concentration at these two sites (Fig. 3). Although model underestimates AOD at Huimin site with the MB of -0.22, both observation and model result show that the AOD at Huimin site is highest among the four sites. Considering the location of Huimin site in Figure 1, this indicates that model can reproduce the more serious pollution to the south of Beijing province.

In addition, in the supplement file, the comparison of AOD from MODIS observations and the corresponding model results shows that model can reproduce the

more pollutants over the south part of Hebei Province and the evolution of AOD values; the comparison of aerosol extinction coefficient from Cloud-Aerosol Lidar and Infrared Pathfinder Satellite Observations (CALIPSO) and the modeled aerosol extinction coefficient shows that model also can capture the vertical distribution and the evolution of aerosol extinction coefficient during the fog-haze period (10–15 January).

4.2 Aerosol impacts on surface energy, meteorological variables, and atmospheric stability

In this section, the aerosol raditive forcing (ARF) and its impacts on surface energy, temperature, RH, atmospheric stability, wind, and PBLH during the fog-haze period (10–15 January) with the simulated maximum surface $PM_{2.5}$ concentration of ~600 ug m^{-3}, minimum atmospheric visibility of ~0.3 km and 10–100 hours of simulated hourly surface $PM_{2.5}$ concentration above 300 ug m^{-3} over NCP are presented. Beijing, Tianjin, and south Hebei Province [BTH region, (36.2 °–41 °N, 114 °–118 °E), black box in Fig. 1] is the key high-aerosol-concentration region over the NCP where there may be significant impacts of aerosol on meteorological variables in the atmospheric boundary layer. Figure 6 is the time series of aerosol-induced daily and diurnal change in the surface energy budget [latent heat (LH), sensible heat (SH), shortwave (SW) radiation, longwave (LW) radiation, and net energy flux (LH+LW+SH+SW)] and meteorological variables (temperature at 2m, RH at 2m) averaged for the BTH region, which is calculated by subtracting the model results of EXP_NOEF from those of EXP_CTL. The diurnal change is calculated for 10–15 January, the pollution episode. Positive values indicate more energy flux toward the surface, or reduced energy flux away from the surface. Figure 6a shows that during 2–26 January, the SW fluxes at the surface are reduced by 8–

36 W m^{-2} due to aerosol scattering and absorption of solar radiation at the surface. The SW fluxes are reduced by 25–35 W m^{-2} during 10–15 January. The LW fluxes are increased slightly by up to 6 W m^{-2} during 2–26 January, with values of 4–6 W m^{-2} during 10–15 January, due to the positive radiative forcing in the atmospheric by aerosol. Because of the cooling effect of aerosol at the surface, the LH and SH fluxes from the surface to the atmosphere during 2–26 January are also reduced by 1–5 W m^{-2} and 5–16 W m^{-2}, respectively. The net energy fluxes at the surface are reduced by 15–50 W m^{-2}, with values of 39–47 W m^{-2} during 10–15 January. Therefore, during the fog-haze period, the energy arriving at the surface was largely reduced. In Fig. 6c, the diurnal change shows the change of surface energy is significant during the daytime: during 10–15 January, at 09:00–18:00, aerosol reduces SW fluxes, LH fluxes, and SH fluxes by 10–105, 2–16, and 9–46 W m^{-2} respectively, and increases LW fluxes by 2–10 W m^{-2}; while during the nighttime, aerosol only increases the LW flux from the atmosphere to the surface by ~3 W m^{-2}. The net surface energy decreases by 6–156 W m^{-2} during 09:00–18:00 and increases by a slightly positive value of around ~1.5 W m^{-2} during 00:00–07:00 and 18:00–23:00, which may lead to surface cooling during the daytime.

For the daily variation of aerosol-induced 2m temperature and 2m RH, in Fig. 6b, averaged for the BTH region, aerosols induce a reduction of surface temperature by 0.2–1.3 ℃ during 2–26 January, with values of 0.8–1.3 ℃ during 10–15 January, the largest reduction during 2–26 January. Aerosols slightly lead to an increase of the surface RH by 0.5–4% during 2–26 January. For the diurnal change depicted in Fig. 6d, it can be seen that the reduction of surface temperature is at a maximum of 0.7–1.1 ℃ during 09:00–18:00, but remains at around 0.6 ℃ during 00:00–08:00 and 19:00–23:00. The aerosol-

induced surface RH increases by 2–5% during 09:00–18:00, but by only 1–2% during 00:00–08:00 and 19:00–23:00. In general, the changes in meteorological variables take place mainly during the daytime (09:00–18:00).

Figure 7 is the spatial distribution of ARF at the bottom of the atmosphere and in the atmosphere and the aerosol impacts on 2m temperature and 2m RH, calculated by subtracting the model results of EXP_NOEF from those of EXP_CTL averaged during 09:00–18:00, 10–15 January. From Fig. 7a, the ARF at the bottom is highest over south Hebei Province and Tianjin, with values of −80 to −140 W m^{-2}, and ranges from −60 to −100 W m^{-2} over south Beijing. Che et al. (2014) analyzed observations at several sites over the NCP during January 2013 and indicated that the daily ARF during 10–15 January at the surface was about −50 to −75 W m^{-2} over north Beijing, and about −100 to −150 W m^{-2} over south Beijing and Hebei Province. These results are to some extent consistent with the model results in Fig. 7a. Contrary to the significant negative ARF at the bottom, the ARF in the atmosphere in Fig. 7b shows that there is a large positive ARF with the value of 40 to 120 W m^{-2} over south Hebei Province and Tianjin, and 20 to 80 W m^{-2} over south Beijing. Therefore, a more stable atmosphere is expected. In Fig. 7c, the aerosol-induced surface temperature decreases most over Tianjin and south Hebei Province, with values of −1.6 to −2.8 ℃. The temperature also decreases by about 0.4 to 1.6 ℃ over Beijing and other parts of Hebei Province. Such a reduction of temperature is a reflection of the decrease in solar radiation reaching the earth's surface due to aerosols. In Fig. 7c, the aerosol-induced surface RH increases by about 8–14% over south Hebei Province, by 4–6% over Tianjin, and by 2–4% over Beijing. As the aerosol-induced change in water vapor mixing ratio is very small (1–2%) over the NCP area (figure not

shown), the decrease in temperature can lead to a decrease in the saturation pressure of water vapor and an increase in RH at the surface, which is beneficial for the hygroscopic growth of aerosols. Figure 8 is the time–altitude distribution of the diurnal cycle of aerosol impacts on temperature and RH averaged for the BTH region during 10–15 January. In Fig. 8a it can be seen that, consistent with Fig. 7a, the temperature decreases near the surface (under 950hPa), with the highest reduction (0.5–1.5 ℃) during 09:00–18:00, while it increases by 0.1–0.5 ℃ between 950 hPa and 850 hPa during 11:00–16:00. Such a change in temperature can increase the stability of the atmosphere during daytime. For RH (Fig. 8b), similar to the change at the surface, its change is opposite to the change in temperature, increasing by about 2–4% under 950 hPa and decreasing by about 1–6% between 950 hPa and 850 hPa during 09:00–20:00.

From the above discussion, the aerosol-induced change of the solar radiation and meteorological variables may change the stability of the atmosphere during the fog-haze event. The profile of the equivalent potential temperature (EPT) can be used to characterize the stability of the atmosphere. Figure 9 is the aerosol impact on EPT profiles at 00:00, 06:00, 12:00, and 18:00, averaged during 10–15 January in the BTH region. As seen in Fig. 9, the impact of aerosol on EPT does not change too much with altitude at 00:00 and 06:00: the EPT decreases by up to around 0.7 K under 950 hPa. At 12:00, aerosol decreases the EPT near the surface (under 925 hPa) by up to around 1.3 K, and increases it between 925 hPa and 750 hPa by up to 0.12 K. This suggests that, at 12:00, aerosol leads to a more stable atmosphere. Aerosol decreases EPT by up to around 1.1 K under 875 hPa at 18:00.

As a results of the more stable atmosphere, Fig. 10 shows the diurnal variation of surface $PM_{2.5}$ concentration from EXP_CTL and aerosol-induced 10m wind speed and PBLH change. In Fig. 10, averaged for the BTH region, the aerosol-induced surface wind speed decreases during 09:00–18:00, with values of 0.1–0.34 m s^{-1} (3–10%), while there is no change at other times of the night. The maximum decrease of wind speed is during 14:00–16:00. The decrease of surface wind speed is not favorable for the diffusion of air pollutants. The PBLH decreases by 22–207 m (8–32%) during 09:00–17:00, with the maximum reduction (17–32%) seen during 13:00–16:00. The large decrease of PBLH is beneficial for the accumulation of the air pollutant. It is noticed that the surface $PM_{2.5}$ concentration is lowest during 11:00–16:00. This indicates that the changed meteorological condition will have the largest impacts on the lowest $PM_{2.5}$ concentration.

4.3 Feedback of aerosol-induced meteorological variables changes to aerosol concentration

The above changes in meteorological variables as a result of aerosol effects (e.g. the decrease of temperature at the surface and the increase of temperature in the middle atmosphere, the increase of RH at the surface and in the lower atmosphere, the more stable atmosphere and the decrease in wind speed and PBLH) can have impacts on the surface $PM_{2.5}$ concentration and eventually contribute to the maintenance and deterioration of regional air pollution. Figures 11a, c, and e show the hourly surface $PM_{2.5}$ concentration from EXP_NOEF and the impacts of changes in meteorological variables on hourly surface $PM_{2.5}$ concentration averaged for the three sub-regions of the BTH (Beijing, Tianjin and Hebei, three boxes with blue dash lines in Fig. 1) during 2–26 January. The corresponding diurnal change during 10–15 January are shown in Fig. 11b,

d, and f. The change in percentage is calculated by comparing with the surface $PM_{2.5}$ concentration from EXP_NOEF. Among the three sub-regions of the BTH, surface $PM_{2.5}$ concentration is highest over Hebei. It can be seen that the maximum increase of meteorological-variables-change-induced surface $PM_{2.5}$ concentration is around 50 μg m^{-3} (70%), 90 μg m^{-3} (60%), and 80 μg m^{-3} (40%) for Beijing, Tianjin, and Hebei, respectively, during 10–15 January. For the average differences between Beijing, Tianjin and Hebei, the higher the surface $PM_{2.5}$ concentration is, the greater the increase is in the surface $PM_{2.5}$ concentration produced by unfavorable meteorological conditions. Note that the time when the maximum increase in surface $PM_{2.5}$ concentration occurs is not the time when the maximum surface $PM_{2.5}$ concentration occurs. Averaged during 10–15 January, the diurnal changes in surface $PM_{2.5}$ concentration in Fig. 11b, d, and f show that the increase in surface $PM_{2.5}$ concentration starts from 09:00, with values of 6–28 μg m^{-3} (10–25%), 10–35 μg m^{-3} (7–20%), 10–35 μg m^{-3} (7–15%) for Beijing, Tianjin, and Hebei, respectively. The surface $PM_{2.5}$ concentration is maximum at around 08:00 and 20:00 and minimum during 10:00–16:00, while the maximum increase in surface $PM_{2.5}$ concentration occurs at 10:00 and 16:00. The feedback of meteorological variables change to surface $PM_{2.5}$ concentration is significant during 09:00–18:00, and thus increases the average value and weakens the daily variation of surface $PM_{2.5}$ concentration.

Figure 12a shows the impact of changes in meteorological variables on the spatial distribution of surface $PM_{2.5}$ concentration averaged during 09:00–18:00, 10–15 January. Consistent with Fig. 11, the meteorological-variables-change-induced increase of surface $PM_{2.5}$ concentration is maximum over Tianjin and south Hebei Province, with values of

30–50 μg m^{-3}; in south Beijing, the values range from 10 to 40 μg m^{-3}. Figure 12b shows that the corresponding surface $PM_{2.5}$ concentration change in percentage terms is higher over southeast Beijing and north Tianjin with the value of 15–30% while is 2–15% over south Hebei Province, south Tianjin and north Beijing. It can be concluded that aerosol induces a more stable atmosphere, which is favorable for the accumulation of air pollutants, and thus contributes to the formation of fog-haze events. A mechanism of positive feedback exists between aerosol concentration and aerosol-induced meteorological conditions.

5.Conclusion

Heavy particulate pollution and fog-haze events over the NCP have drawn much attention recently. In this paper, we estimate the feedback between atmospheric aerosols and meteorological variables during a fog-haze period in January 2013. This is achieved by conducting numerical simulations using a coupled meteorology and aerosol/chemistry model (WRF-Chem). The period from 10–15 January, when the NCP experienced a severe fog-haze event, is analyzed in detail. Major conclusions are as follows.

The spatial and temporal characteristics of temperature, RH, wind, surface $PM_{2.5}$ concentration, visibility and AOD during 2–26 January 2013 is reproduced by the simulation using the fully-coupled WRF-Chem model.

The results of the numerical experiments show that, averaged during 09:00–18:00, 10–15 January, aerosols lead to a significant negative radiative forcing of -20–-140 W m^{-2} at the surface and a large positive radiative forcing of 20–120 W m^{-2} in the atmosphere and the temperature decreases by 0.8–2.8 ℃ at the surface and increases by 0.1–0.5 ℃ at

around 925 hPa while the RH increases by about 4–12% at the surface and decreases by 1–6% at around 925 hPa. The maximum change occurs over urban Beijing and Tianjin, and south Hebei Province. As a result, the aerosol-induced equivalent potential temperature profile change shows that the atmosphere is much more stable and thus the surface wind speed decreases by up to 0.3 m s^{-1} (10%) and the atmosphere boundary layer height decreases by 40–200 m (5–30%) during the daytime of this severe fog-haze event.

The results of the numerical experiments also show that, due to such a more stable atmosphere, compared to the surface $PM_{2.5}$ concentration from the model results without aerosol feedback, the maximum increase of hourly surface $PM_{2.5}$ concentration is around 50 μg m^{-3} (70%), 90 μg m^{-3} (60%), and 80 μg m^{-3} (40%) in Beijing, Tianjin, and south Hebei Province, respectively, during 10–15 January. The surface $PM_{2.5}$ concentration averaged during 09:00–18:00, 10–15 January, over the NCP, increases by 10–50 μg m^{-3}, with the maximum change taking place over urban Beijing and Tianjin, and south Hebei Province. Although the aerosol concentration is maximum during the nighttime, the feedback mechanism by which meteorological variables increase the aerosol concentration most occurs during daytime (at around 10:00 and 16:00). These results suggest that aerosol induces a more stable atmosphere, which is favorable for the accumulation of air pollutants, and thus contributes to the formation of fog-haze events. A mechanism of positive feedback exists between aerosol concentration and aerosol-induced meteorological conditions.

There are uncertainties in this study. The model overestimates $PM_{2.5}$ at Xianghe and Tianjin according to Figure 3. The diurnal variation of $PM_{2.5}$ at Xianghe and Tianjin from

model results and observations shows that the overestimation is basically at night which may relate to the setting of atmospheric boundary layer height at night in the model and also the bias of emission inputted to the model. As the aerosol feedback derived from the aerosol radiative effect mainly has large impacts during daytime, it is noted that the overestimation of $PM_{2.5}$ may lead to slight overestimation of the aerosol feedback during the pollutant period. Emission with higher resolution may be useful for improving the model performance. The aerosol direct and indirect effect is also very sensitive to the mixing state between scattering aerosols and absorbing aerosols. Moreover, the feedback between aerosol and cloud/meteorological parameters also has large uncertainty. Although aerosol indirect forcing is considered in WRF-Chem, it only includes the aerosol effect on resolved stratiform clouds. With a horizontal resolution of 27 km, convective clouds are still parameterized in the model without explicit cloud microphysics in the convective cloud parameterization that links aerosols to cloud condensation or ice nuclei.

Acknowledgements

This work was supported by the National Basic Research Program of China (2014CB953802), the "Strategic Priority Research Program (B)" of the Chinese Academy of Sciences (XDB05030105, XDB05030102, XDB05030103), the International S&T Cooperation Program of China (2011DFG23450), the National Natural Science Foundation of China (41305010) and the Russian Scientific Fund under grant 14-47-00049.

References

Abdul-Razzak, H., and Ghan, S.J.: A parameterization of aerosol activation 2. Multiple aerosol types, J. Geophys. Res., 105(D5), 6837–6844, 2000.

Albrecht, B.A.: Aerosols, cloud microphysics, and fractional cloudiness, Science, 245, 1227–1230, 1989.

Barndard, J.C., Fast, J.D., Paredes-Miranda, G., Arnott, W.P., and Laskin, A.: Technical Note: Evaluation of the WRF-Chem "Aerosol Chemical to Aerosol Optical Properties" Module using data from the MILAGRO campaign, Atmos. Chem. Phys., 10, 7325–7340, 2010.

Brown, J.F., Loveland, T.R., Merchant, J.W., Reed, B.C., and Ohlen, D.O.: Using multi-source data in global land-cover characterization: concepts, requirements, and methods, Photogram. Eng. Rem. S., 59, 977–987, 1993.

Chan, C.K., and Yao, X.: Air pollution in mega cities in China, Atmos. Environ., 42, 1–42, 2008.

Che, H., Xia, X., Zhu, J., Li, Z., Dubovik, O., Holben, B., Goloub, P., Chen, H., Estelles, V., Cuevas-Agulló, E., Blarel, L., Wang, H., Zhao, H., Zhang, X., Wang, Y., Sun, J., Tao, R., Zhang, X., and Shi, G.: Column aerosol optical properties and aerosol radiative forcing during a serious haze-fog month over North China Plain in 2013 based on ground-based sunphotometer measurements, Atmos. Chem. Phys., 14, 2125–2138, 2014.

Che, H., Zhang, X., Chen, H., Damiri, B., Goloub, P., Li, Z., Zhang, X.,Wei, Y., Zhou, H., Dong, F., Li, D., and Zhou, T.: Instrument calibration and aerosol optical depth validation of the China Aerosol Remote Sensing Network, J. Geophys. Res., 114, D03206, doi:10.1029/2008JD011030, 2009a.

Che, H., Zhang, X., Li, Y., Zhou, Z., and Qu, J.J.: Horizontal visibility trends in China 1981-2005, Geophys. Res. Lett., 34, L24706, doi:10.1029/2007GL031450, 2007.

Che, H., Zhang, X., Li, Y., Zhou, Z., Qu, J., and Hao, X.: Haze trends over the capital cities of 31 provinces in China, 1981-2005, Theor. Appl. Climatol., 97, 235–242, 2009b.

Cheng, S., Yang, L., Zhou, X., Xue, L., Gao, X., Zhou, Y., and Wang, W.: Size-fractionated water-soluble ions, situ PH and water content in aerosol on hazy days and the influences on visibility impairment in Jinan, China, Atmos. Environ., 45, 4631–4640, 2011.

Deng, X. J., Tie, X., Wu, D., Zhou, X. J., Tan, H. B., Li, F., and Jiang, C.: Long–term trend of visibility and its characterizations in the Pearl River Delta Region (PRD), China, Atmos. Environ., 42, 1424–1435, 2008.

Dubovik, O., Holben, B., Eck, T.F., Smirnov, A., Kaufman, Y.J., King, M.D., Tanre, D., and Slutsker, I.: Variability of absorption and optical properties of key aerosol types observed in worldwide locations, J. Atmos. Sci., 59, 590-608, 2002.

Dubovik, O., and King, M.D.: A flexible inversion algorithm for retrieval of aerosol optical properties from Sun and sky radiance measurements, J. Geophys. Res., 105, 20673-20696, 2000.

Fast, J.D., Gustafson, Jr. W.I., Easter, R.C., Zaveri, R.A., Barnard, J.C., Chapman, E.G., and Grell, G.A.: Evolution of ozone, particulates, and aerosol direct forcing in an urban area using anew fully-coupled meteorology, chemistry, and aerosol model, J. Geophys. Res., 111, D21305, doi:10.1029/2005JD006721, 2006.

Feng, S., Hu, S.Q., and Qian, W.H.: Quality control of daily meteorological data in China, 1951–2000: A new dataset, Int. J. Climatol., 24, 853–870, 2004.

Gao, Y., and Zhang, M.: Numerical Simulation of a Heavy Fog-Haze Episode over the North China Plain in January 2013, Climatic Environ. Res. (in Chinese), 19(2), 140–152, 2014.

Ghan, S.J., Easter, R.C., Hudson, J., and Breon, F.-M.: Evaluation of Aerosol Indirect Radiative Forcing in MIRAGE, J. Geophys. Res., 106, 5317–5334, 2001a.

Ghan, S., Laulainen, N., Easter, R., Wagener, R., Nemesure, S., Chapman, E., Zhang, Y., and Leung, R.: Evaluation of aerosol direct radiative forcing in MIRAGE, J. Geophys. Res., 106, 5295–5316, 2001b.

Gong, S.L.: A parameterization of sea-salt aerosol source function for sub- and super-micron particles, Global Biogeochem. Cycles, 17, 1097, doi:10.1029/2003GB002079, 2003.

Gong, S.L., Barrie, L.A., and Blanchet, J.-P.: Modeling sea-salt aerosols in the atmosphere, J. Geophys. Res., 102, 3805–3818, 1997.

Grell, G.A., Peckham, S.E., Schmitz, R., McKeen, S.A., Frost, G., Skamarock, W.C., and Eder, B.: Fully coupled "online" chemistry within the WRF model, Atmos. Environ., 39, 6957–6975, 2005.

Guenther, A., Karl, T., Harley, P., Wiedinmyer, C., Palmer, P.I., and Geron, C.: Estimates of global terrestrial isoprene emissions using MEGAN (Model of Emissions of Gases and Aerosols from Nature), Atmos. Chem. Phys., 6, 3181–3210, 2006.

Gustafson, Jr W.I., Chapman, E.G., Ghan, S.J., Easter, R.C., and Fast, J.D.: Impact on modeled cloud characteristics due to simplified treatment of uniform cloud condensation nuclei during NEAQS 2004, Geophys. Res. Lett., 34, L19809, doi:10.1029/2007GL030021, 2007.

Han, X., Zhang, M., Tao, J., Wang, L., Gao, J., Wang, S., and Chai, F.: Modeling aerosol impacts on atmospheric visibility in Beijing with RAMS-CMAQ, Atmos. Environ., 72, 177–191, 2013.

He, K. B.: Multi-resolution Emission Inventory for China (MEIC): model framework and 1990-2010 anthropogenic emissions, International Global Atmospheric Chemistry Conference, 17-21 September, Beijing, China, 2012.

Holben, B.N., Eck, T.F., Slutsker, I., Tanre, D., Buis, J. P., Setzer, A., Vermote, E., Reagan, J.A., Kaufman, Y.J., Nakajima, T., Lavenu, F., Jankowiak, I., and Smirnov, A.: AERONET--A federated instrument network and data archive for aerosol characterization, Remote Sens. Environ., 66, 1-16, 1998.

Hsu, N.C., Jeong, M.J., Bettenhausen, C., Sayer, A.M., Hansell, R., Seftor, C.S., Huang, J., and Tsay, S.C.: Enhanced Deep Blue aerosol retrieval algorithm: The second generation, J. Geophys. Res., 118(16), 9296–9315, 2013.

Huang, Y., Dickinson, R.E., and Chameides, W.L.: Impact of aerosol indirect effect on surface temperature over East Asia, Proc. Natl. Acad. Sci., 103, 4371–4376, doi:10.1073/pnas.0504428103, 2006.

Jaeglé, L., Quinn, P.K., Bates, T.S., Alexander, B., and Lin, J.-T.: Global distribution of sea salt aerosols: new constraints from in situ and remote sensing observations, Atmos. Chem. Phys., 11, 3137–3157, doi:10.5194/acp-11-3137-2011, 2011.

Lei. Y., Zhang, Q., He, K.B., and Streets, D.G.: Primary anthropogenic aerosol emission trends for China, 1990–2005, Atmos. Chem. Phys., 11, 931–954 http://dx.doi.org/10.5194/acp-11-931-2011, 2011.

Li, Z., Xia, X., Cribb, M., Mi, W., Holben, B., Chen, H., Wang, P., Tsay, S.-C., Eck, T. F., Zhao, F., Dutton, E.G., and Dickerson, R.E.: Aerosol optical properties and its radiative effects in northern China, J. Geophys. Res., 112, D22S01, doi:10.1029/2006JD007382, 2007.

Liu, H., Zhang, L., and Wu, J.: A Modeling Study of the Climate Effects of Sulfate and Carbonaceous Aerosols over China, Adv. Atmos. Sci., 27, 1276–1288, 2010.

Liu, J., Xia, X., Wang, P., Li, Z., Zheng, Y., Cribb, M. and Chen, H.: Significant aerosol direct radiative effects during a pollution episode in northern China, Geophys. Res. Lett., 34, L23808, doi:10.1029/2007GL030953, 2007.

Liu, Y., Daum, P.H., and McGraw, R.: Size Truncation Effect, Threshold Behavior, and a New Type of Autoconversion Parameterization, Geophys. Res. Lett., 32, L11811, doi:10.1029/2005GL022636, 2005.

Loveland, T.R., Merchant, J.W., Ohlen, D.O., and Brown, J.F.: Development of a land-cover characteristics database for the conterminous US, Photogram. Eng. Rem. S., 57, 1453–1463. 1991.

Patashnick, H, and Rupprecht, E.: Continuous PM10 measurements using the tapered element oscillating microbalance, J Air Waste Manage., 41, 1079–1083. 1991.

Petters, M.D., and Kreidenweis, S.M.: A single parameter representation of hygroscopic growth and cloud condensation nucleus activity, Atmos. Chem. Phys., 7, 1961–1971, doi:10.5194/acp-7-1961-2007, 2007.

Qian, Y., Leung, L.R., Ghan, S.J., and Giorgi, F.: Regional climate effects of aerosols over China: Modeling and observation, Tellus B, 5I5, 914–934, 2003.

Quan, J., Zhang, Q., He, H., Liu, J., Huang, M., and Jin, H.: Analysis of the formation of fog and haze in North China Plain (NCP), Atmos. Chem. Phys., 11, 8205-8214, doi:10.5194/acp-11-8205-2011, 2011.

Ramanathan, V., Crutzen, P.J., Kiehl, J.T., and Rosenfeld, D.: Aerosols, climate, and the hydrological cycle, Science 294, 2119–2124, 2001.

Randerson, J.T., Van der Werf, G.R., Giglio, L., Collatz, G.J., and Kasibhatla, P.S.: Global Fire Emissions Database, Version 2 (GFEDv2.1). Available at http://daac.ornl.gov/ (last access: 11 November 2013) from Oak Ridge National Laboratory Distributed Active Archive Center, Oak Ridge, Tennesse, USA, doi:10.3334/ORNLDAAC/849, 2005.

Skamarock, W.C., Klemp, J.B., Dudhia, J., Gill, D.O., Barker, D.M., Duda, M., Huang, X.-Y., Wang, W., and Powers, J.G.: A description of the Advanced Research WRF version 3.Tech. Rep. NCAR/TN-475+STR, 113 pp, 2008, Boulder, Colorado, USA.

Streets, D.G., Bond, T.C., Carmichael, G.R., Fernandes, S.D., Fu, Q., He, D., Klimont, Z., Nelson, S.M., Tsai, N.Y., Wang, M.Q., Woo, J.-H., and Yarber, K.F.: An inventory of gaseous and primary aerosol emissions in Asia in the year 2000, J. Geophys. Res. 108(D21), 8809, doi:10.1029/2002JD003093, 2003.

Sun, Y., Jiang, Q., Wang, Z., Fu, P., Li, J., Yang, T., and Yin, Y.: Investigation of the Sources and Evolution Processes of Severe Haze Pollution in Beijing in January 2013, J. Geophys. Res. 114(7), 4380–4398, 2014.

Sun, Y., Zhuang, G., Tang, A., Wang, Y., and An, Z.: Chemical characteristics of PM2.5 and PM10 in Haze-Fog episodes in Beijing, Environ. Sci. Technol., 40, 3148–3155, 2006.

Tao, M., Chen, L., Xiong, X., Zhang, M., Ma, P., Tao, J., and Wang, Z.: Formation process of the widespread extreme haze pollution over northern China in January 2013:

implications for regional air quality and climate, Atmos. Environ., 98, 417-425, doi: 10.1016/j.atmosenv.2014.09.026, 2014.

Twomey, S.: Pollution and the planetary albedo, Atmos. Environ., 8, 1251–1256, 1974.

Wang, H., Tan, S.C., Wang, Y., Jiang, C., Shi, G.Y., Zhang, M.X., and Che, H.Z.: A multisource observation study of the severe prolonged regional haze episode over eastern China in January 2013, Atmos. Environ., 89, 807–815, 2014b.

Wang, Y.S., Yao, L., Wang, L.L., Liu, Z., Ji, D., Tang, G., Zhang, J., Sun, Y., Hu, B., and Xin, J.: Mechanism for the formation of the January 2013 heavy haze pollution episode over central and eastern China, Sci. China Earth Sci., 57, 14–25, doi: 10.1007/s11430-013-4773-4, 2014a.

Wang, S., Zhao, M., Xing, J., Wu, Y., Zhou, Y., Lei, Y., He, K., Fu, L., and Hao, J.: Quantifying the air pollutants emission reduction during the 2008 Olympic games in Beijing, Environ. Sci. Technol., 44, 2490–2496, 2010.

Wu, J., Fu, C., Xu, Y., Tang, J., Han, Z. and Zhang, R.: Effects of total aerosol on temperature and precipitation in East Asia, Clim. Res., 40, 75–87, 2009.

Wu, P., and Han, Z.: Indirect radiative and climatic effects of sulfate and organic carbon aerosols over East Asia investigated by RIEMS, Atmos. Oceanic Sci. Lett., 4, 7–11, 2011.

Xia, X., Li, Z., Wang, P., Chen, H., and Cribb, M.: Estimation of aerosol effects on surface irradiance based on measurements and radiative transfer model simulations in northern China, J. Geophys. Res., 112, D22S10, doi:10.1029/2006JD008337, 2007.

Yu, M., Carmichael, G.R., Zhu, T., Cheng Y.F.: Sensitivity of predicted pollutant levels to urbanization in China, Atmos. Environ., 60, 544-554, 2012.

Zaveri, R.A., Easter, R.C., Fast, J.D., and Peters, L.K.: Model for simulating aerosol interactions and chemistry (MOSAIC), J. Geophys. Res., 113, D13204, doi:10.1029/2007JD008792, 2008.

Zhang, J.K., Sun, Y., Liu, Z.R., Ji, D.S., Hu, B., Liu, Q., Wang, Y.S.: Characterization of submicron aerosols during a month of serious pollution in Beijing, 2013, Atmos. Chem. Phys., 14 (6), 2887–2903, 2014.

Zhang, Q., Streets, D.G., Carmichael, G.R., He, K., Huo, H., Kannari, A., Klimont, Z., Park, I.S., Reddy, S., Fu, J.S., Chen, D., Duan, L., Lei, Y., Wang, L., and Yao, Z.: Asian emissions in 2006 for the NASA INTEX-B mission, Atmos. Chem. Phys., 9, 5131–5153, 2009.

Zhang, X., Wang, Y., Niu, T., Zhang, X., Gong, S., Zhang, Y., and Sun, J.: Atmospheric aerosol compositions in China: Spatial/temporal variability, chemical signature, regional

haze distribution and comparisons with global aerosols, Atmos. Chem. Phys., 12, 779–799, doi:10.5194/acp-12-779-2012, 2012.

Zhao, C., Liu, X., Leung, L.R., and Hagos, S.: Radiative impact of mineral dust on monsoon precipitation variability over West Africa, Atmos. Chem. Phys., 11, 1879–1893, 2011.

Zhao, C., Liu, X., Leung, L.R., Johnson, B., McFarlane, S.A., Gustafson, Jr W.I., Fast, J.D., and Easter, R.C.: The spatial distribution of mineral dust and its shortwave radiative forcing over North Africa: modeling sensitivities to dust emissions and aerosol size treatments, Atmos. Chem. Phys., 10, 8821–8838, 2010.

Zhao, X.J., Zhao, P.S., Xu, J., Meng, W., Pu, W.W., Dong, F., He, D., and Shi, Q.F..: Analysis of a winter regional haze event and its formation mechanism in the North China Plain, Atmos. Chem. Phys., 13, 5685–5696, 2013.

Table 1. Statistics of the comparisons between simulated and observed temperature (℃), relative humidity (RH, %), wind speed (m s^{-1}), surface $PM_{2.5}$ concentration (μg m^{-3}), visibility (km), and aerosol optical depth (AOD) during 2–26 January 2013.

		[a]N	[b]C_{OBS}	[b]C_{MOD}	[c]R	[d]MB	[d]NMB(%)	[e]RMSE
Temperature	BJ	25	−5.0	−5.5	0.78	−0.5	9.0	1.6
	MY	25	−7.7	−7.6	0.91	0.1	−2.0	1.3
	BD	25	−6.5	−6.0	0.86	0.5	−7.2	1.3
	TS	25	−7.7	−7.6	0.91	0.1	−0.7	1.3
	TJ	25	−5.3	−6.9	0.88	−1.6	31.2	2.1
	QHD	25	−7.9	−7.6	0.83	0.3	−3.4	1.5
RH	BJ	25	57.6	57.1	0.72	−0.4	−0.7	12.6
	MY	25	64.3	63.6	0.84	−0.7	−1.0	10.5
	BD	25	77.5	69.1	0.87	−8.4	−10.8	11.0
	TS	25	70.9	69.9	0.76	−1.0	−1.4	9.6
	TJ	25	64.2	74.4	0.90	10.3	16.0	12.8
	QHD	25	67.5	71.7	0.78	4.1	6.1	8.8
WS	BJ	25	1.7	2.2	0.82	0.5	27.8	0.82
	MY	25	1.6	2.8	0.64	1.2	78.7	1.4
	BD	25	1.8	2.6	0.83	0.75	40.8	1.0
	TS	25	2.1	3.1	0.68	1.0	46.4	1.3
	TJ	25	2.2	2.9	0.65	0.7	30.9	1.2
	QHD	25	2.0	3.8	0.51	1.9	100.0	2.1
$PM_{2.5}$	BJ	600	138.4	123.4	0.63	-15.1	-10.9	102.8
	XL	590	49.1	62.0	0.69	12.9	26.2	44.8
	XH	502	139.8	181.2	0.56	41.4	29.6	113.9
	TJ	500	135.9	216.9	0.69	80.9	59.5	124.9
Visibility	BJ	100	11.2	16.2	0.77	5.0	44.5	10.3
	TJ	100	8.0	8.1	0.66	0.1	0.95	6.0
	BD	100	6.5	7.2	0.58	0.7	10.5	5.8
	SJZ	100	5.8	5.7	0.43	-0.1	-2.8	5.1
AOD	BJ	22	0.52	0.42	0.59	−0.10	−20.2	0.34
	XL	12	0.23	0.34	0.99	0.11	47.2	0.12
	XH	16	0.64	0.41	0.60	−0.23	−36.7	0.47
	Huimin	18	0.96	0.73	0.74	−0.22	−23.3	0.50

[a] *N* is the number of paired samples;
[b] C_{OBS} and C_{MOD} are the monthly average values of observation and model results, sampled at the observation site and time, respectively;
[c] *R* is the correlation coefficient between the observation and model results;
[d] *MB* and *NMB* are the mean biases between the observation and model results, and the normalized mean bias between the observation and model results, respectively;
[e] *RMSE* is the root-mean-square error between observation and model results.

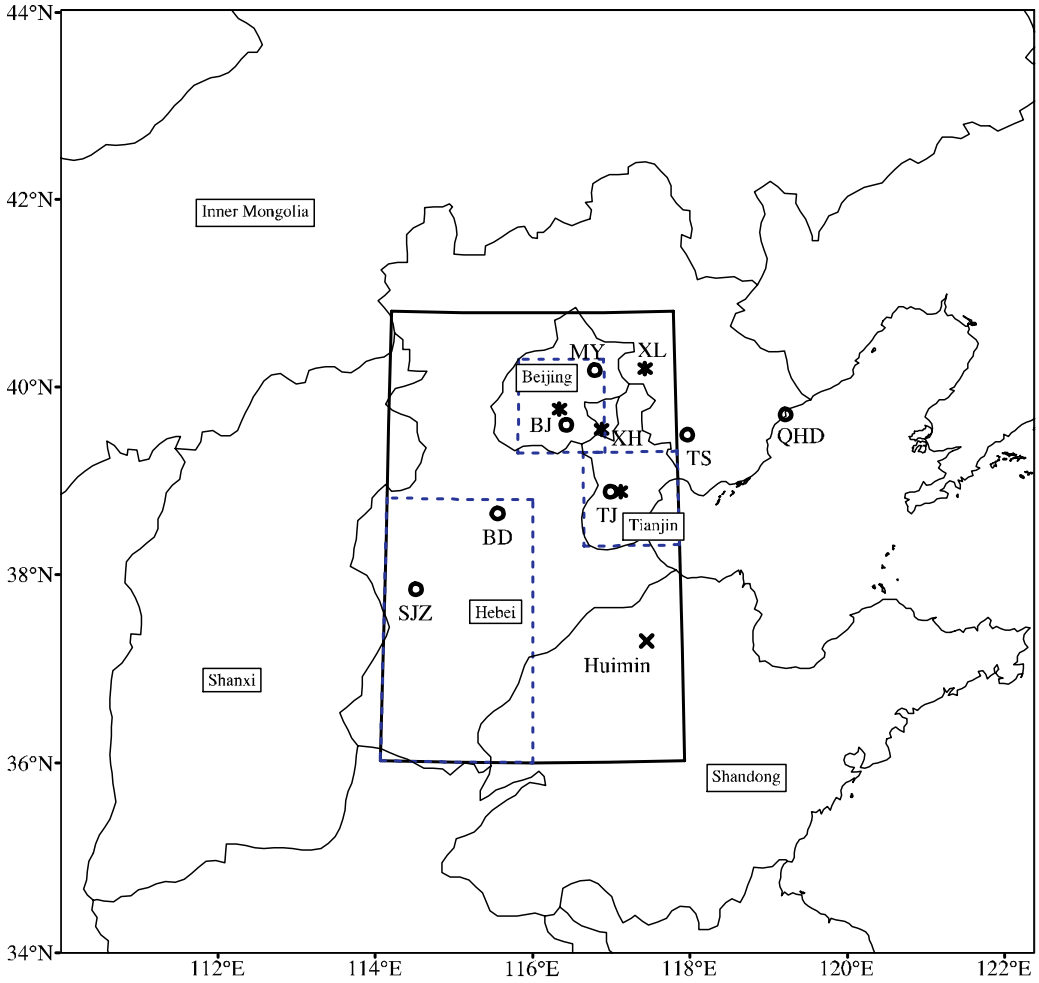

Figure 1. Study domain and regional divisions: Hebei Province, Beijing, Tianjin, Inner Mongolia, Shanxi Province, and Shandong province. The observation sites (BJ, MY, BD, TS, TJ, QHD and SJZ) from CNMC are denoted as circles and those from the CARE-China network (BJ, TJ, XH and XL) are denoted as stars, of which BJ and TJ from CNMC and the CARE-China network are very close. The observation sites (BJ, XL and XH) from AERONET have the same locations as those from CARE-China. Huimin site from Che et al. (2014) is denoted as a cross. The black box denotes the region of Beijing, Tianjin and Hebei Province (BTH region, 36.2°–41°N, 114°–118°E), and the three blue boxes with dashed lines denote Beijing, Tianjin and south Hebei Province, respectively.

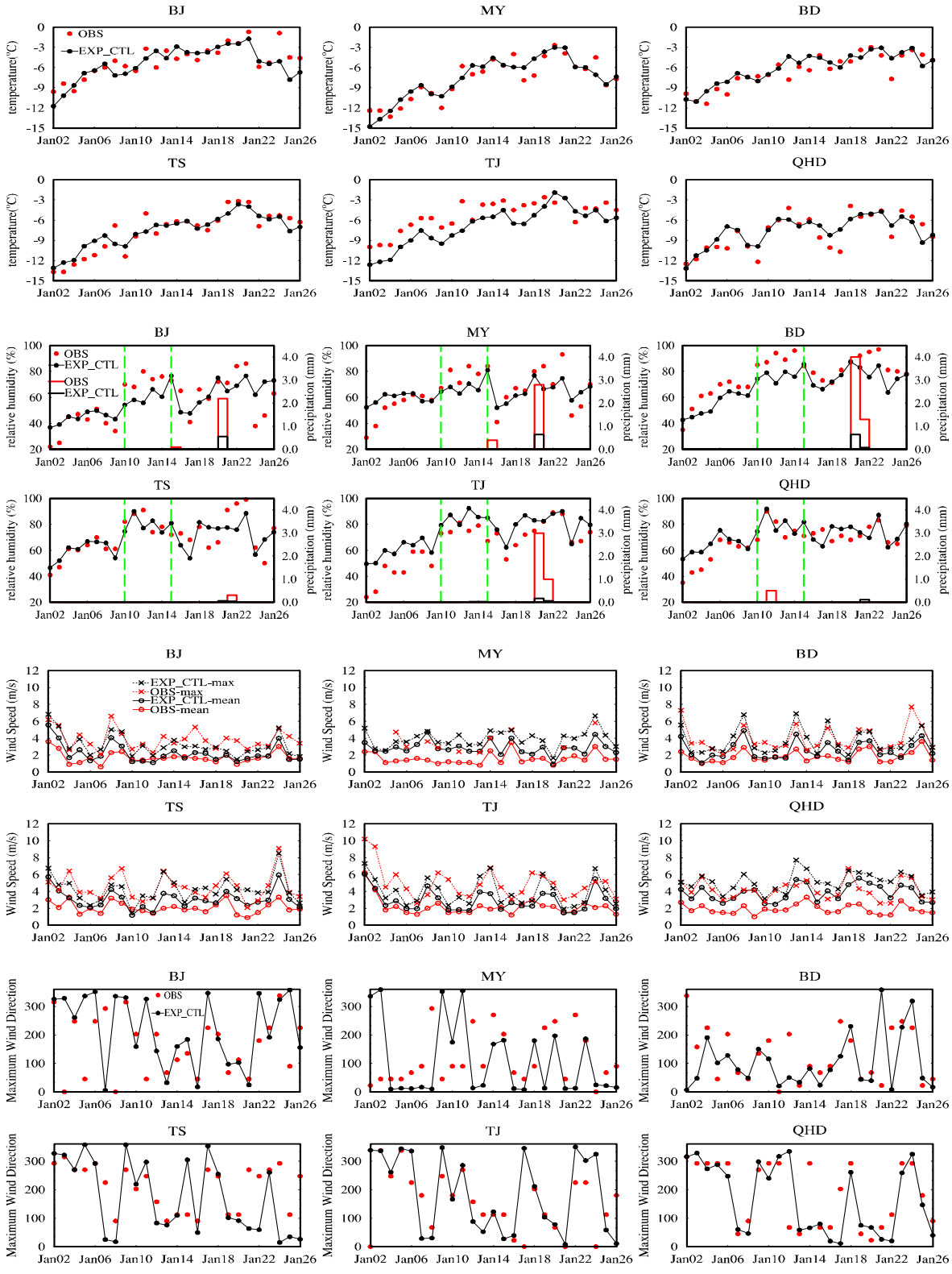

Figure 2. Time series of observed (red) and simulated (black, EXP_CTL) daily-averaged 2m temperature (℃), daily-averaged 2m relative humidity (%), daily precipitation (mm,

bar), daily-averaged 10m wind speed (m s^{-1}, solid line), daily 10m maximum wind speed (dashed line) and daily wind direction of maximum wind speed at BJ, MY, BD, TS, TJ and QHD during 2–26 January 2013.

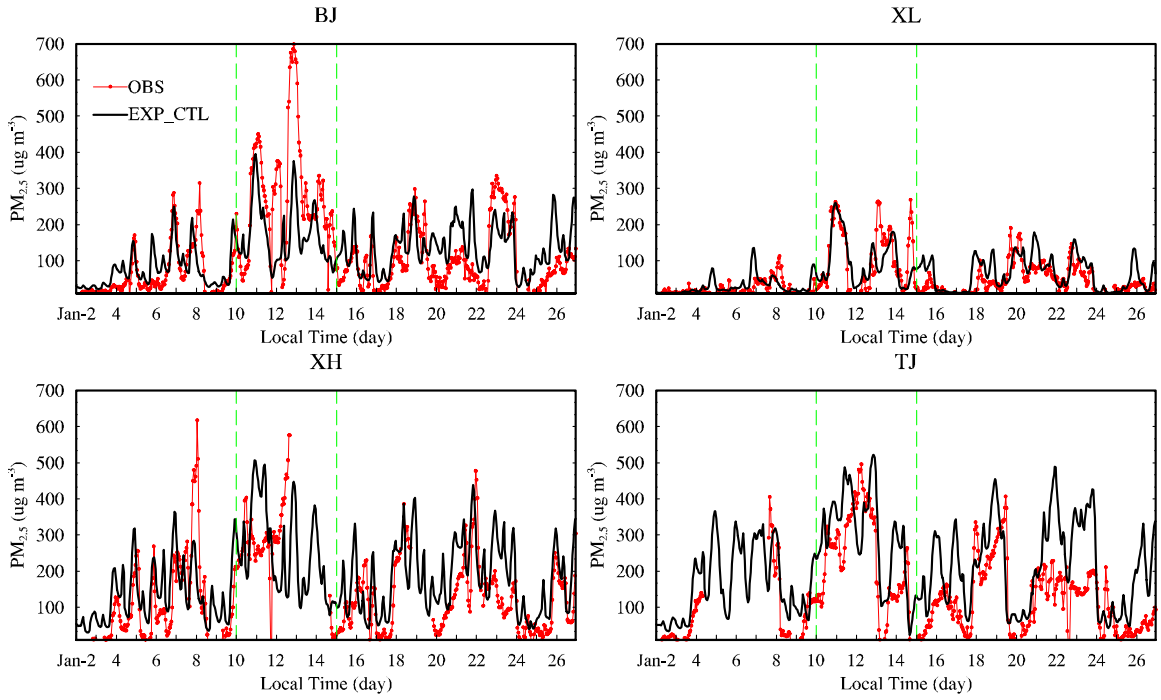

Figure 3. Time series of hourly surface $PM_{2.5}$ concentration (μg m^{-3}) from the CARE-China network measurement and the corresponding WRF-Chem simulation (EXP_CTL) at BJ, XL, XH and TJ during 2–26 January 2013.

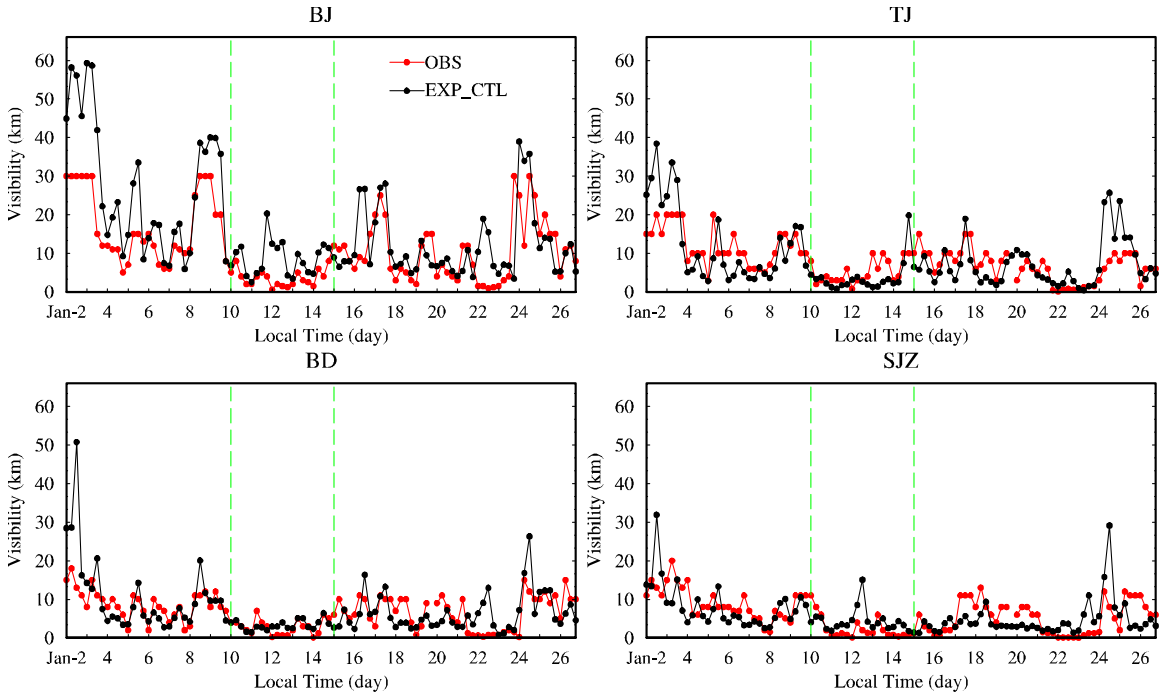

Figure 4. Time series of hourly visibility (km) at 00:00, 06:00, 12:00, 18:00 from CNMC measurements and the corresponding WRF-Chem simulation (EXP_CTL) at BJ, TJ, BD and SJZ during 2–26 January 2013.

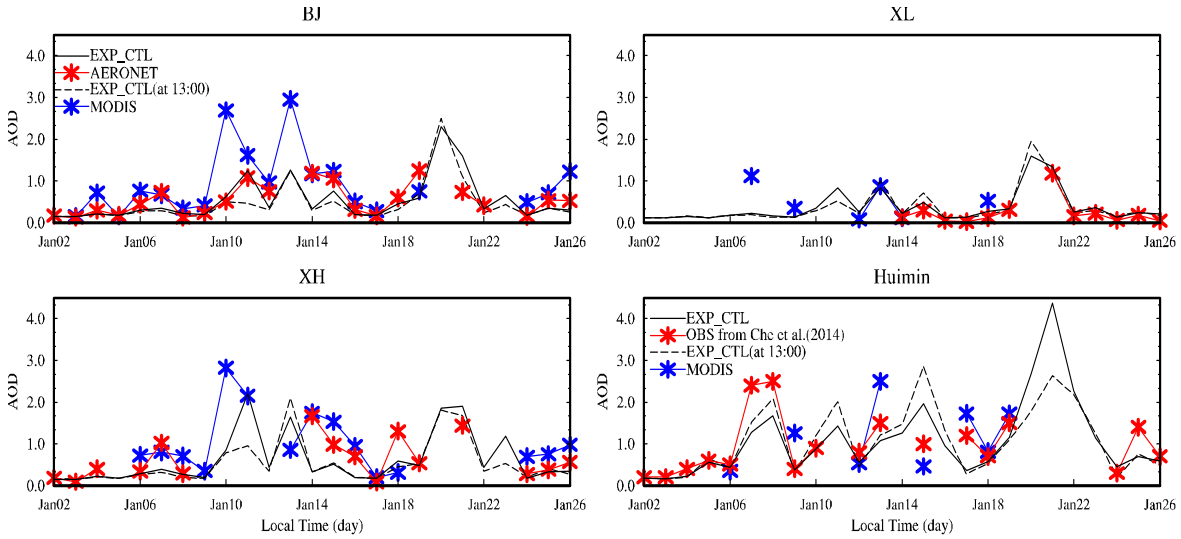

Figure 5. Time series of daily AOD at 550 nm from AERONET measurements at BJ, XL and XH site and from Che et al. (2014) at Huimin site (daily average) and MODIS retrievals (at 13:00 local time) and the corresponding WRF-Chem simulation (EXP_CTL) for daily average (solid black line) and at 13:00 local time (dash black line) during 2–26 January 2013.

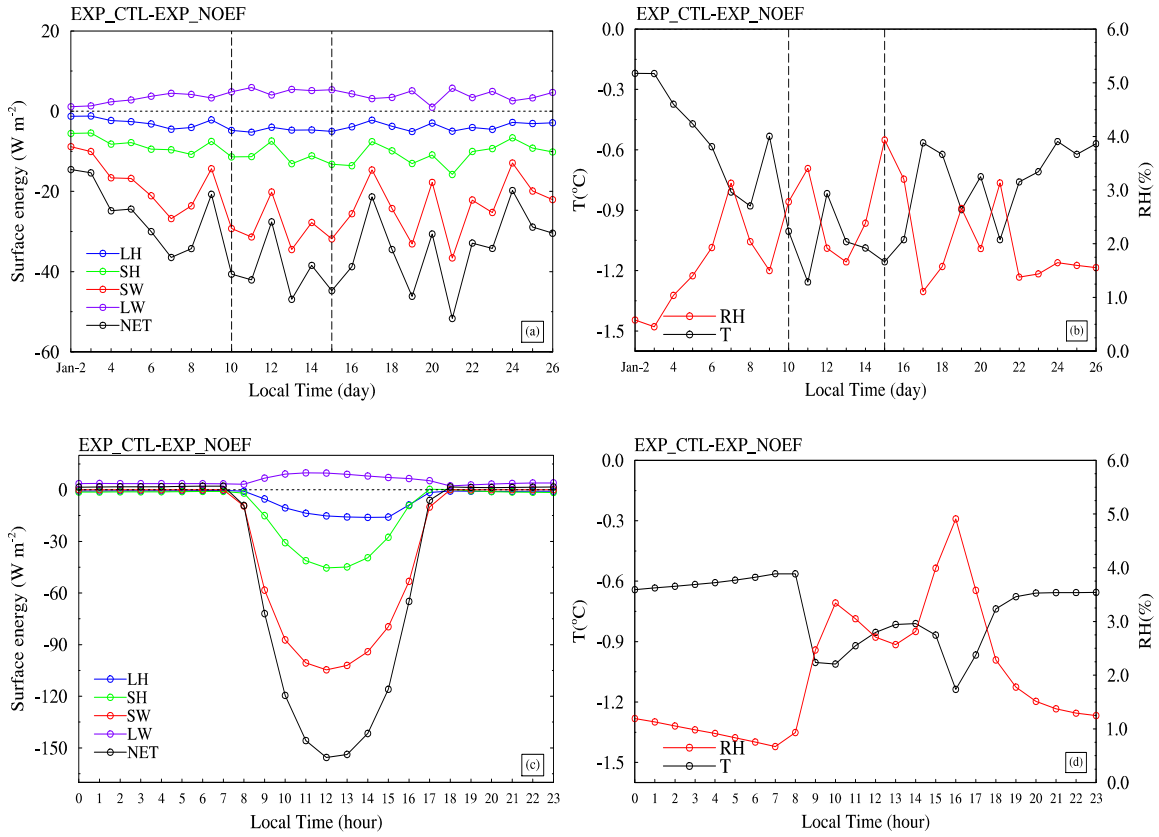

Figure 6. Time series of aerosol-induced daily change in (a) surface energy budget (SH, LH, LW radiation, SW radiation, and net energy flux, W m^{-2}) and (b) meteorological variables [2m temperature (℃), 2m RH(%)] averaged for the BTH region (36°–42°N,113°–120°E) during 2–26 January. Time series of aerosol-induced diurnal change of (c) surface energy budget and (d) meteorological variables averaged for the BTH region and the period 10–15 January 2013. LH is latent heat, LW is longwave radiation, SH is sensible heat, SW is shortwave radiation, and NET is the sum of the total energy fluxes.

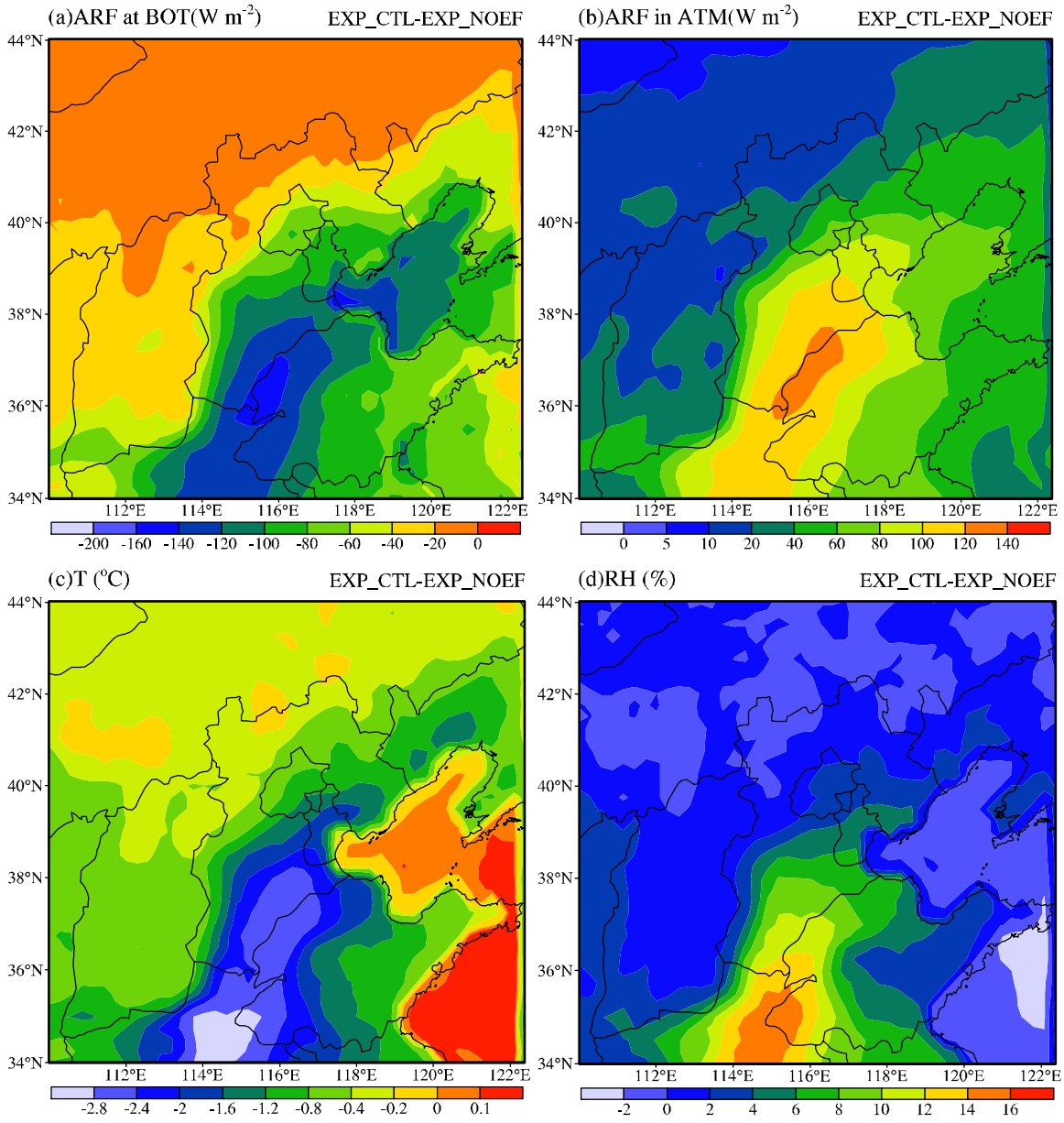

Figure 7. Spatial distribution of aerosol radiative forcing (ARF, W m^{-2}) (a) at bottom and (b) in the atmosphere and the aerosol-induced change in (c) 2m temperature (℃) and (d) 2m RH (%) averaged during 09:00–18:00, 10–15 January 2013.

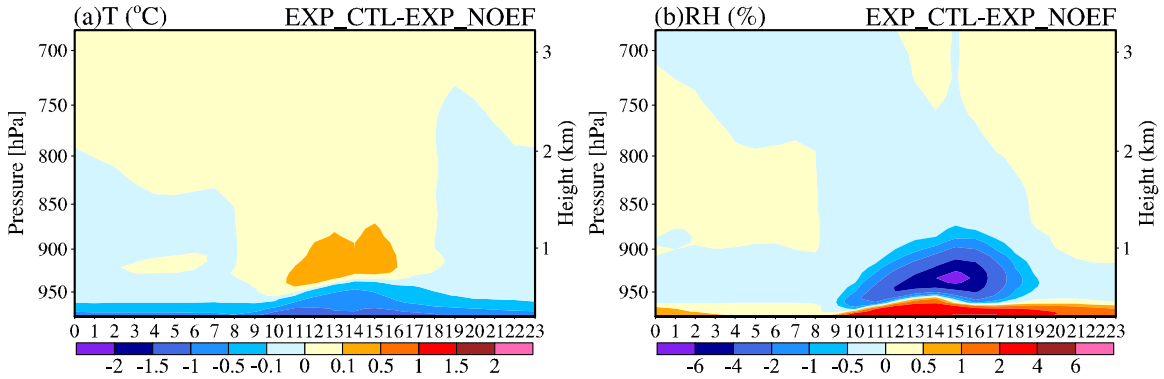

Figure 8. Time–altitude distribution of aerosol-induced diurnal change in (a) temperature (℃) and (b) RH (%) averaged for the BTH region and the period 10–15 January 2013.

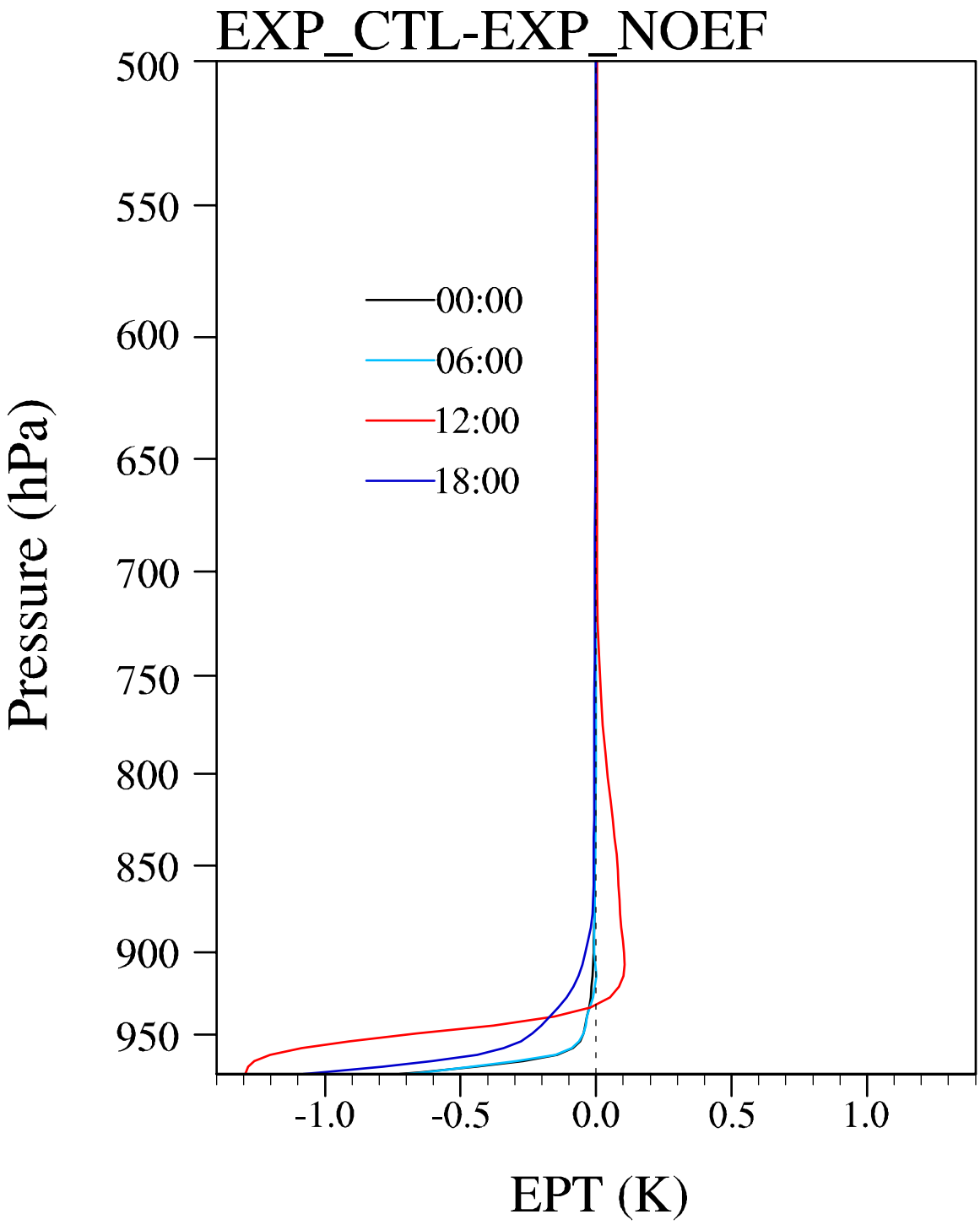

Figure 9. Aerosol impact on equivalent potential temperature (EPT, K) profiles at 00:00, 06:00, 12:00 and 18:00 averaged for the BTH region and the period 10–15 January 2013.

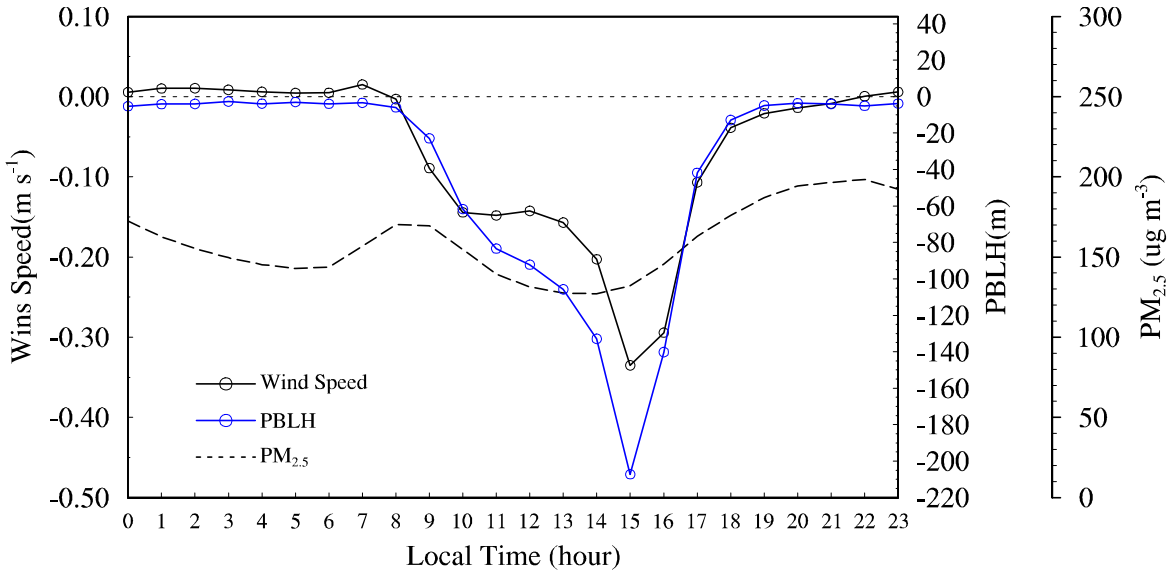

Figure 10. Time series of diurnal variation of surface $PM_{2.5}$ concentration from EXP_CTL and aerosol-induced diurnal change of wind speed (m s^{-1}) and PBLH (m) averaged for the BTH region and the period 10–15 January 2013.

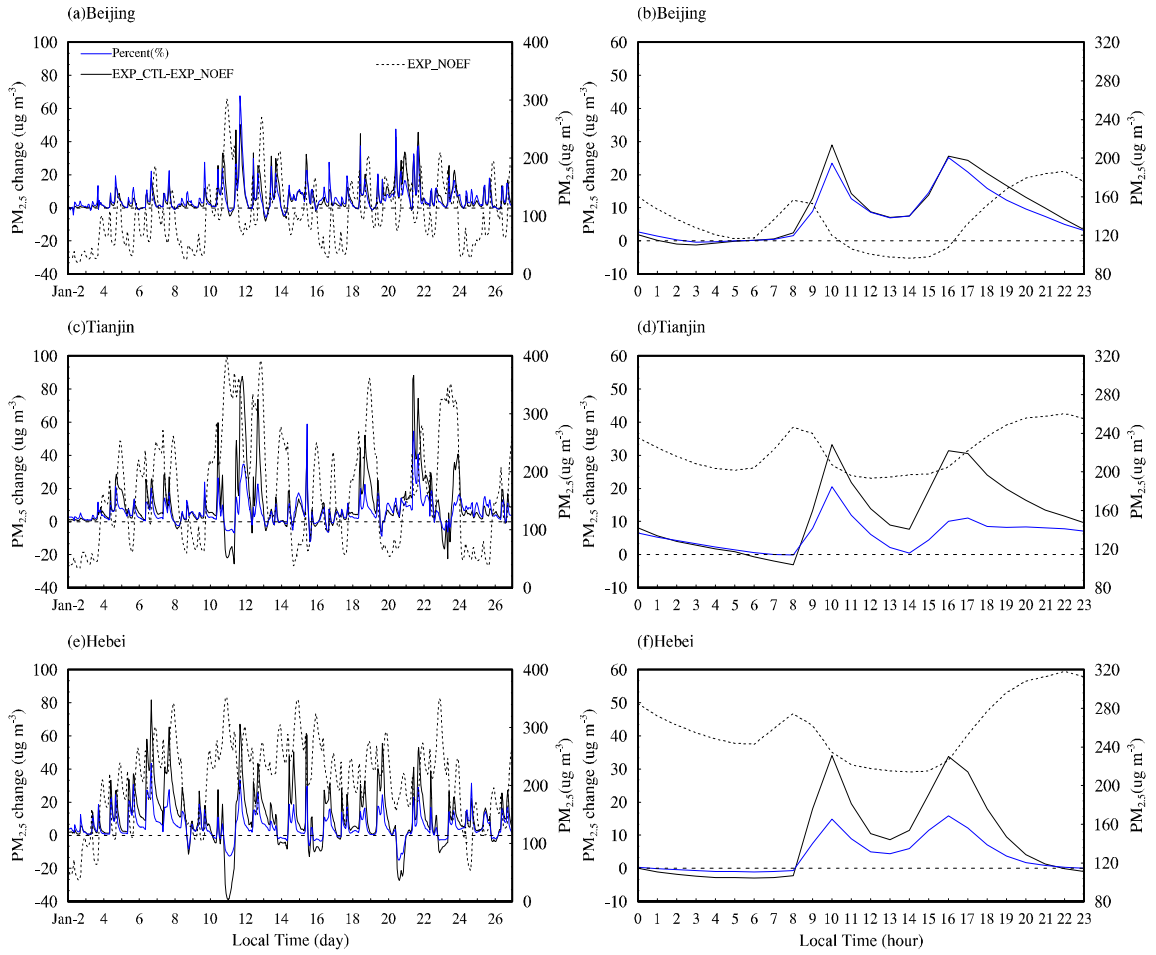

Figure 11. Time series of surface $PM_{2.5}$ concentration from EXP_NOEF and the meteorological-variables-change-induced hourly surface $PM_{2.5}$ concentration (μg m^{-3}) change averaged for (a) Beijing, (c) Tianjin and (e) Hebei during 2–26 January and the corresponding diurnal change averaged for (b) Beijing, (d) Tianjin and (f) Hebei during 10–15 January 2013. The black solid line denotes the change value of surface $PM_{2.5}$ concentration and the blue solid line denotes the corresponding change in percentage terms compared to the surface $PM_{2.5}$ concentration from the model results of EXP_NOEF. Beijing, Tianjin and Hebei comprise the BTH region (dashed blue boxes in Figure 1).

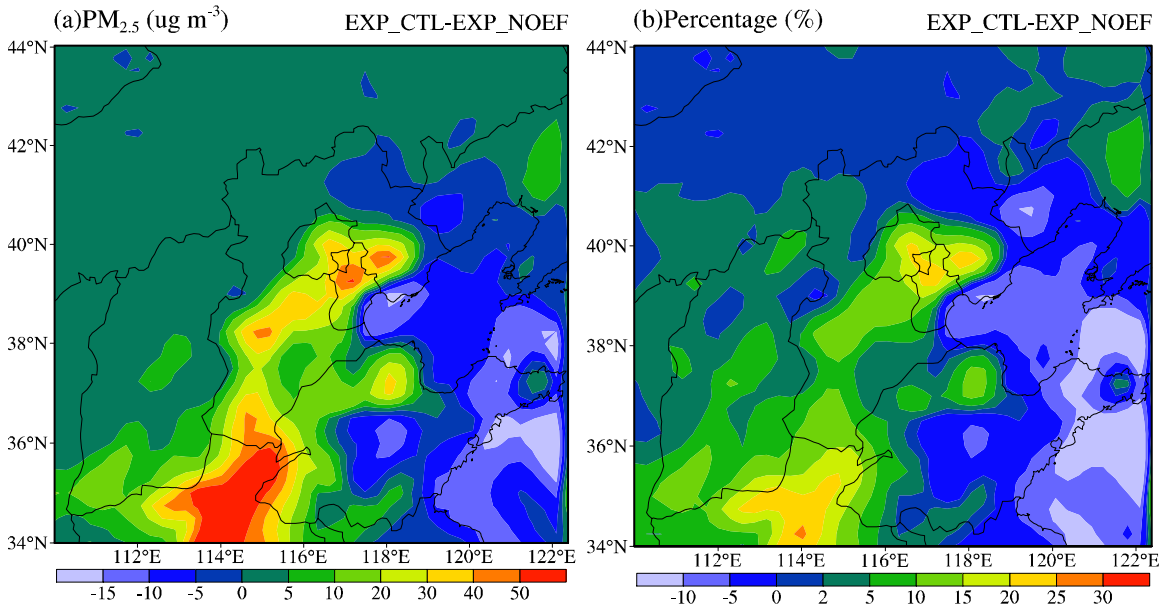

Figure 12. (a) Spatial distribution of the meteorological-variables-change-induced surface $PM_{2.5}$ concentration change (μg m^{-3}) averaged during 09:00–18:00, 10–15 January 2013. Panel (b) shows the change in percentage terms compared to the surface $PM_{2.5}$ concentration from the model results of EXP_NOEF.